nature portfolio

Peer Review File

Manipulatable Cascade Pumping Single-Photon Upconversion

Corresponding Author: Professor Bin Dong

This file contains all reviewer reports in order by version, followed by all author rebuttals in order by version.

Version 0:

Reviewer comments:

Reviewer #1

(Remarks to the Author)
This work developed a machine learning-guided single-photon cascade pumping strategy that simplified conventional upconversion from a multi-step energy transfer process to a single-photon process on a "virtual ground state". In the $NaYS_2$:Ho^{3+} system, RGB emissions were selectively enhanced by 2–3 orders of magnitude, response time drops from 30 ms to 54 μs, and the upconversion response extended to ~2100 nm. It also achieved high-sensitivity, fast-response narrowband photodetection at ~2100 nm for CO_2 sensing. The structure of the paper is well organized and the data are relatively comprehensive, but the following issues still need to be further addressed:
1. The alphabetical order in the legend of Figure 4 is incorrect.
2. Why was $NaYS_2$ chosen as the matrix in this study? What are the advantages of $NaYS_2$ over the commonly used $NaYF_4$?
3. In the dual-wavelength cascade pumping scheme, why was the 2096 nm laser operated in continuous wave (CW) mode while the 980 nm laser was operated in pulsed mode? Why not the opposite (i.e., 980 nm CW and 2096 nm pulsed)? If the wavelength difference between the two lasers is reduced, would the observed phenomena still occur?
4. Is there a correlation between the emission wavelength of $NaYS_2$:Ho^{3+} under 980 & 2096 nm dual-wavelength excitation and the excitation frequency of the 980 nm pulsed wavelength? Please provide the corresponding experimental data.

Reviewer #2

(Remarks to the Author)
Upconversion, which converts near-infrared photons into easily detectable visible photons, is an ideal approach for infrared detection. However, current upconversion still faces critical bottlenecks such as limited effective excitation wavelength, low quantum efficiency, and slow response speed. Dong et al. proposed a cascade pumping strategy to achieve single-photon upconversion, using appropriate multi-wavelength matching to target energy levels for efficient upconversion emission while circumventing complex energy losses. In NaYS2:Ho^{3+}, the response wavelength was extended to 2096 nm, the emission intensity was enhanced by more than three orders of magnitude, and the rise time was significantly reduced to the microsecond level. Importantly, this strategy is generalizable to other Ln3+ systems and enables narrowband infrared detection at 2096 nm and high-sensitivity CO2 sensing via a photo-assisted approach.

I anticipate that this work is very interesting, and will have high academic impact for the development of upconversion luminescent materials and high-performance optoelectronic devices. Furthermore, the manuscript is well-structured and clearly presented; therefore, I recommend it for publication in Nature Communications. A few minor points are listed below:

1. Machine learning: What nearest-neighbor search strategy does the algorithm employ during the numerical screening stage? When no satisfying nearest neighbor or valid combination exists, what is the algorithm's fault-tolerance mechanism?
2. This LEGO-stacking single-photon upconversion model is generalizable. The authors should establish upconversion rate equations to verify which factors the emission enhancement depends on.
3. Under cascade pumping, the red emission intensity enhancement factor (×4220) of the NaYS2:1%Ho3+ system is significantly higher than that of other Ho3+ singly doped systems with different concentrations. The paper should clarify why the NaYS2:1%Ho3+ system exhibits a higher enhancement factor.
4. The long-term stability data of the photoresponse devices are of positive significance. The authors should supplement the changes in photocurrent values of the upconversion PDs under prolonged illumination, which would help verify its robustness in practical applications.

5. The gas detection application is based on laser absorption spectroscopy, using a CO_2/N_2 gas mixture. The authors should also provide the absorption curve of N_2 to demonstrate that it exhibits no significant absorption at 2004 nm.

Reviewer #3

(Remarks to the Author)
This work describes a dual wavelength excitation approach to achieve high efficiency emission from upconversion materials at discrete red/green and blue wavelengths. The authors claim to use a machine learning approach to inform the ideal combinations of excitation wavelength to produce optimal emission at the each wavelengths. They then go on to experimentally validate their predictions and demonstrate the application of their dual wavelength excitation methodology for gas and CO_2 sensing in combination with suitable photodetectors.

The work is certainly interesting and presents a simple and elegant approach to achieving efficient visible light emission from upconverting (UC) lanthanide ions. It constitutes a significant advancement in the field of photon UC with broad applicability into other disciplines. I therefore recommend publication in Nature Communications after some minor revisions.
A. The machine learning algorithm in Supp Note 1 needs more thorough description and referencing. For example, the statement "…a simple transformation is performed using machine learning algorithms to calculate the corresponding gaps of energy levels." is vague and uninformative.
B. In general it would have been good to increase the discussion around the minimum requirements in the lifetimes of the excited state to function as "virtual ground states". What is this threshold? Are the reported pathways the only possible combinations to produce emission in the RBG regions or are other less efficient pathways also viable?
C. Enhancement factors are often reported, but it is not always clear what they are in reference too. Fig S6 in particular was not clear.
D. The scheme and description of the gas sensing setup is misleading. The reference and detection beams do not produce a new converging pink photon, but rather travel colinear toward the photodetector. The structure of the photodetector, including the deposition of the UC crystals is not suitably described in either the text or SI.
E. Can the authors explain the origin of the reported EQE exceeding 100%?
F. In general, reported for photodetection and CO_2 sensing appear idealised examples and lack evidence of repetition or error ranges.
G. Minor grammatical errors including undefined acronyms (Eg. PD, PCBM) and experimental details are not sufficient for replication (Eg. Excitation intensities in Fig 1e-g and Fig 2h-j, description of the commercial 2004nm PD used for comparison, etc.)

Version 1:

Reviewer comments:

Reviewer #1

(Remarks to the Author)
Authors have well addressed all the reviewers' comments. It is acceptable for publication in this journal.

Reviewer #2

(Remarks to the Author)
Revision is satisfactory and manuscript has been being improved substantially. Therefore, present form of the manuscript can be recommended for the publication.

Reviewer #3

(Remarks to the Author)
The authors have clearly invested significant time and effort to carefully address comments from all the reviewers. I personally am satisfied that they have adequately addressed all my comments and would be happy to see this work published Nature Communications. See point by point below.

(1) Much improved explanation & referencing
(2) Thank you for the clear explanation. Satisfied with the new inclusions
(3) Much clearer now
(4) Satisfied with new figures & corresponding explanations
(5) Satisfied
(6) Excellent inclusion of new data
(7) Satisfied

Details of a point-by-point response to reviewer:

Response to Reviewer #1:

Reviewer #1: This work developed a machine learning-guided single-photon cascade pumping strategy that simplified conventional upconversion from a multi-step energy transfer process to a single-photon process on a "virtual ground state". In the $NaYS_2$:Ho^{3+} system, RGB emissions were selectively enhanced by 2-3 orders of magnitude, response time drops from 30 ms to 54 μs, and the upconversion response extended to ~2100 nm. It also achieved high-sensitivity, fast-response narrowband photodetection at ~2100 nm for CO_2 sensing. The structure of the paper is well organized and the data are relatively comprehensive, but the following issues still need to be further addressed:

(Q1) The alphabetical order in the legend of Figure 4 is incorrect.

Response: We sincerely thank you for your careful comment. According to you suggestion, we have corrected the legend of Figure 4 and have thoroughly rechecked the entire manuscript to avoid similar issues.

(Q2) Why was $NaYS_2$ chosen as the matrix in this study? What are the advantages of $NaYS_2$ over the commonly used $NaYF_4$?

Response: Thank you for your thoughtful and constructive question. Selecting an appropriate host matrix is crucial for achieving efficient cascade pumping single-photon UC, which usually has following properties: i) high efficiency with low phonon energy, ii) large Y^{3+}-Y^{3+} distance with low nonradiative losses, and iii) a long excited-state lifetime of the doped luminescent ions. Compared with typical host materials such as fluorides (e.g., $NaYF_4$) and oxides (e.g., Y_2O_3), $NaYS_2$ possesses a lower phonon energy and long excited-state lifetime of the doped luminescent ions (**Table R1**; [1] Nat. Commun. 2022, 13, 6549; [2] ACS Appl. Mater. Interfaces 2016, 8, 30312; [3] Nat. Commun.2019, 10, 1811; [4] Opt. Mater. 2026, 169, 117595). This characteristic suppresses nonradiative relaxation paths and facilitates the re-stimulation process, thereby enabling efficient cascade pumping UC and allowing precise modulation of excited-state electronic transition dynamics. Considering the above properties, in machine learning screening, $NaYS_2$ stands out as the preferred host material for cascade pumping single-photon UC (Fig 1c).

Table R1 Structure and optical properties comparison of $NaYS_2$, $NaYF_4$ and Y_2O_3.

	$NaYS_2$	$NaYF_4$	Y_2O_3
Phonon energy	278 cm^{-1} [1]	350 cm^{-1} [2]	565 cm^{-1} [2]
Distance (Y^{3+}-Y^{3+})	3.964 Å	3.637 Å	3.516 Å
Excited-state lifetime ($^4I_{13/2}$ of Er^{3+})	~30 ms [1]	~1 ms [3]	~4 ms [4]

To quantitatively verify its superiority, we performed comparative cascade pumping UC experiments using typical fluorides and oxides as reference hosts under same pumping conditions (**Figure R1; Corresponding to the Fig. S12**). The results demonstrate that $NaYS_2$ achieves the best cascade pumping UC enhancement (approximately 4220-fold), significantly outperforming $NaYF_4$ (~1420-fold), Y_2O_3 (~11-fold), and $La_2Mo_2O_9$ (~505-fold). This finding also validates the universality of our cascade pumping single-photon UC approach.

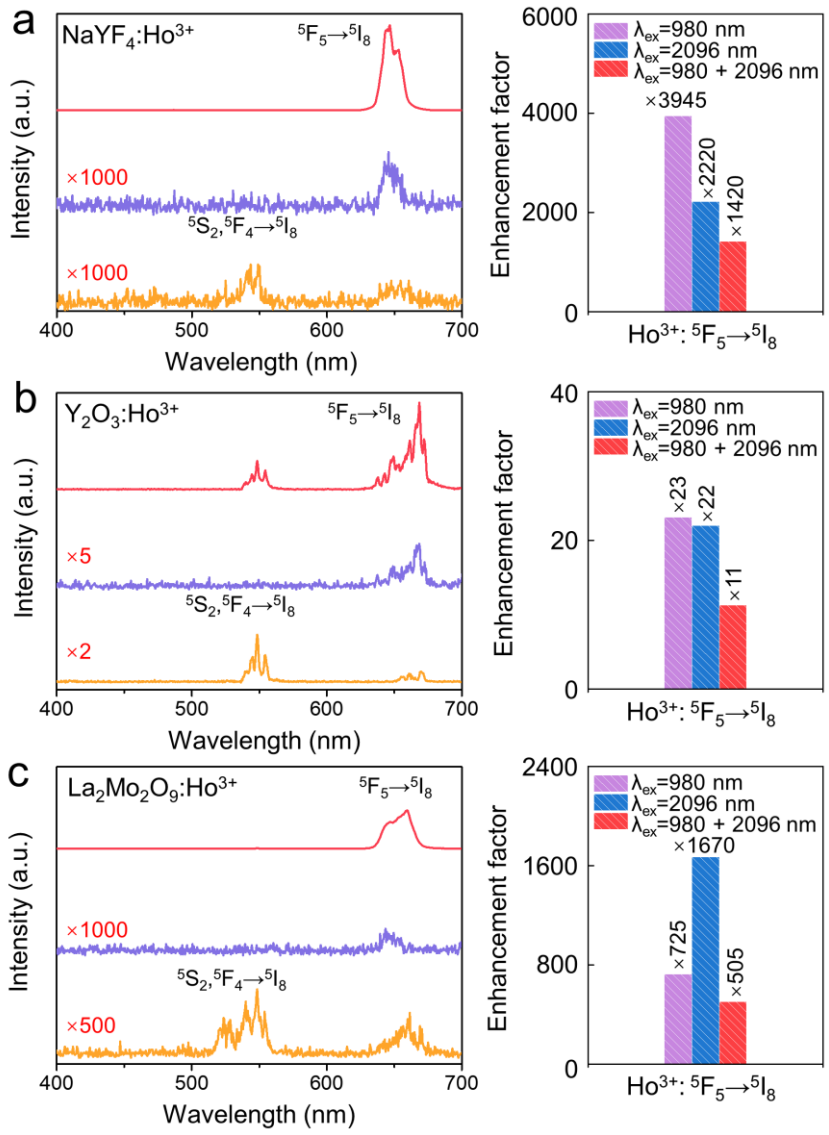

Figure R1 (**Corresponding to the Fig. S12**) The UC emission spectra of (a) $NaYF_4$:1mol%Ho^{3+}, (b) Y_2O_3:1mol%Ho^{3+} and (c) $La_2Mo_2O_9$:1mol%Ho^{3+} under single/dual-wavelength excitation, accompanied by histograms of enhancement multiples compared to different wavelengths (980 nm, 2096 nm and 980 nm + 2096 nm). For the Ho^{3+} $^5F_5 \rightarrow {}^5I_8$ transition (red emission) under cascade excitation of 980 nm & 2096 nm, the red emission intensity is 3945 ($NaYF_4$), 23 (Y_2O_3), 725 ($La_2Mo_2O_9$) times that under 980 nm single excitation, 2220 ($NaYF_4$), 22 (Y_2O_3), 1670 ($La_2Mo_2O_9$) times that under 2096 nm single excitation, and 1420 ($NaYF_4$), 11 (Y_2O_3), 505 ($La_2Mo_2O_9$) times the sum of the two single excitation intensities.

(Q3) In the dual-wavelength cascade pumping scheme, why was the 2096 nm laser operated in continuous wave (CW) mode while the 980 nm laser was operated in pulsed mode? Why not the opposite (i.e., 980 nm CW and 2096 nm pulsed)? If the wavelength difference between the two lasers is reduced, would the observed phenomena still occur?

Response: Thank you for your valuable comments. In fact, dual-wavelength cascade pumping UC is feasible under both pulsed and continuous-wave (C.W.) excitation regimes at each pumping wavelength. Different excitation modes were employed in our studies to better understand the steady-state behavior and dynamics of UC in our system. In the steady-state spectroscopy

measurements, both the 980 nm and 2096 nm lasers were operated in C.W. excitation mode. To measure the UC rise/decay time for the $^5F_5$ energy level, the 980 nm laser was operated in pulsed mode while the 2096 nm laser was operated in C.W. mode. The shortened UC rise time confirms that cascaded pumping single-photon UC can utilize the intermediate excited state as a new "virtual ground state," thereby achieving rapid population of the target energy level.

Regarding your second question, we supplemented the data using the opposite scheme, i.e., pumping with 980 nm C.W. light and 2096 nm pulsed light (**Figure R2; corresponding to Fig. S20**). When using 2096 nm as a P.W. source and 980 nm as a C.W. source, we also observe a reduction in the steady-state time (**Figure R2a; corresponding to Fig. S20a**).In this circumstance, the electron population in the $^5I_7$ state remains unstable due to the intermittent photon supply. Conversely, the second excited state ($^5I_6$) maintains a stable population through continuous 980 nm photon absorption. The subsequent electron transition from $^5I_6$ to $^5F_5$ for Ho^{3+} red UC emission involves a two-photon absorption process of 2096 nm (**Figure R2b; corresponding to Fig. S20b**).

Thus, to better understand the UC populating mechanism, we selected the configuration where the 2096 nm laser was operated in CW mode while the 980 nm laser was operated in pulsed mode.

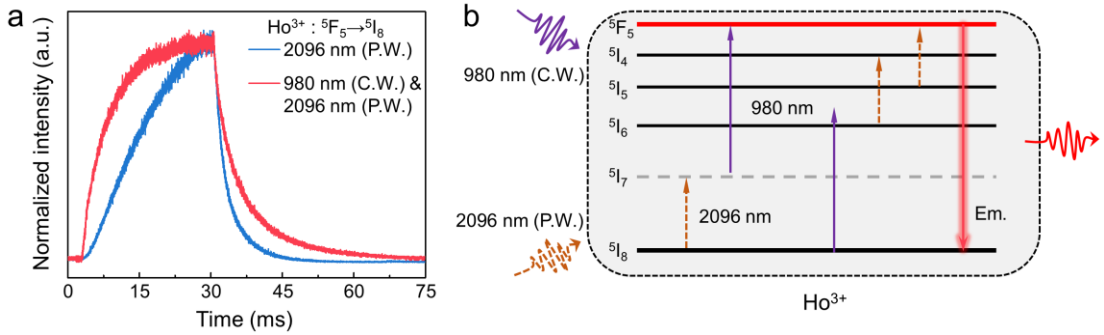

Figure R2 (**Corresponding to the Fig. S20**) (a) Time-dependent red (667 nm) emission profiles of $NaYS_2$:Ho^{3+} under pulsed dual-wavelength excitation with a duration time (pulse width) of 30 ms. 2096 nm laser as P.W. beam; 980 nm laser as C.W. beam. (b) Mechanism model of energy levels for modulation of red UC luminescence upon cascade pumping mode.

Based on the third question, we supplemented our measurements with spectral data recorded under conditions of a reduced wavelength. When using 980 nm and 1208 nm excitation, UC luminescence enhancement can also be observed by appropriately matching the wavelengths to the different energy levels of Ho^{3+} (**Figure R3a; Corresponding to the Fig. S14a**). When the excitation wavelengths (980 nm and 1532 nm) deviate too far from the energy level gap, the cascaded pumping UC luminescence enhancement effect becomes ineffective (**Figure R3b; Corresponding to the Fig. S14c**). Theoretically, the degree of matching between the excitation photons and both the ground state and intermediate level of the luminescent ions directly determines the intermediate-level population efficiency and the UC luminescence performance.

The specific revisions have been incorporated into the manuscript (page 8) and Supplementary Information.

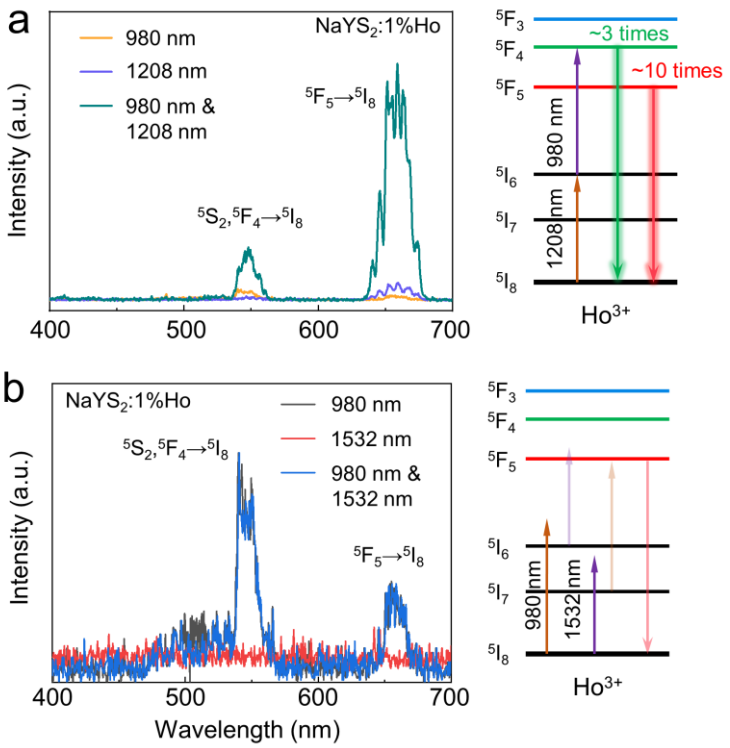

Figure R3 (**Corresponding to the Fig. S14**) The UC emission spectra of $NaYS_2$:Ho^{3+} (1 mol%) under various single/dual-wavelength excitation ((a) 980 nm and 1208 nm; (b) 980 nm and 1532 nm), accompanied with a simple transition mechanism of single-photon infrared UC by LEGO-inspired photon stacking.

(Q4) Is there a correlation between the emission wavelength of $NaYS_2$:Ho^{3+} under 980 & 2096 nm dual-wavelength excitation and the excitation frequency of the 980 nm pulsed wavelength? Please provide the corresponding experimental data.

Response: We appreciate the reviewer's valuable comment. Theoretically, the emission wavelength of rare earth ions is determined by the intrinsic energy level difference of their 4f orbitals and the crystal field environment of the host. As an external time-domain excitation parameter,eg., the pulsed frequency, can alter the populating process but cannot alter the intrinsic emission wavelength of rare earth ions.

According to your suggestion, we further measured the emission spectra under excitation at 980 nm and 2096 nm with varying the repetition frequency of 980 nm pulsed laser from 10 Hz to 500 Hz, as shown in **Figure R4a** (**(corresponding to Fig. S21a**). It shows that the characteristic emission peak at 658 nm corresponding $^5F_5 \rightarrow {}^5I_8$ transition, remains nearly unchanged. In **Figure R4b** (**Corresponding to the Fig. S21b**), we analyzed the red-to-green emission ratio (I_{Red}/I_{Green}) under different pulse frequencies. It was found that as the laser repetition frequency increases, the red-to-green ratio exhibits slight change, indicating that the pulse frequency weak effect onUC populating in our system.

These detailed analyses have been incorporated into the manuscript (page 8) and Supplementary Information.

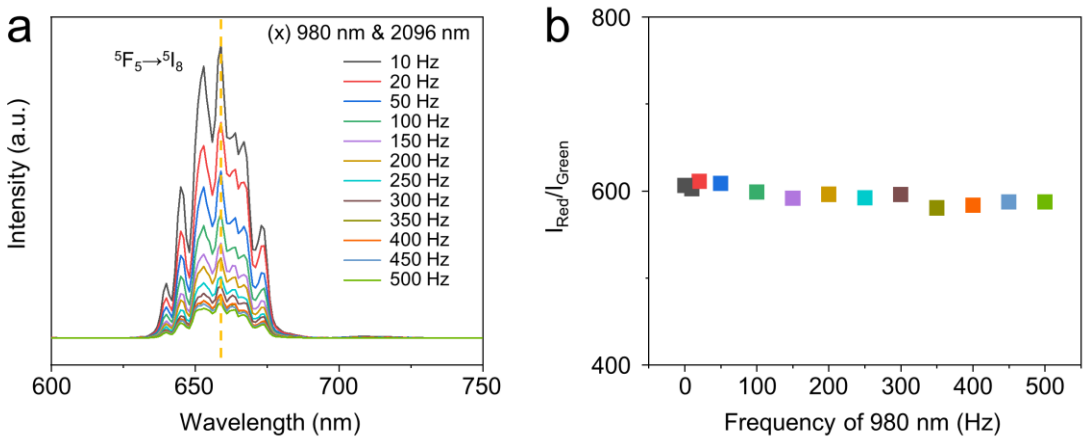

Figure R4 (**Corresponding to the Fig. S21**) (a) The UC emission spectra and (b) I_{Red}/I_{Green} of $NaYS_2:Ho^{3+}$ (1 mol%) under dual-wavelength cascade pumping of 980 nm and 2096 nm with different excitation frequencies.

Response to Reviewer #2:

Reviewer #2: Upconversion, which converts near-infrared photons into easily detectable visible photons, is an ideal approach for infrared detection. However, current upconversion still faces critical bottlenecks such as limited effective excitation wavelength, low quantum efficiency, and slow response speed. Dong et al. proposed a cascade pumping strategy to achieve single-photon upconversion, using appropriate multi-wavelength matching to target energy levels for efficient upconversion emission while circumventing complex energy losses. In $NaYS_2$:Ho^{3+}, the response wavelength was extended to 2096 nm, the emission intensity was enhanced by more than three orders of magnitude, and the rise time was significantly reduced to the microsecond level. Importantly, this strategy is generalizable to other Ln^{3+} systems and enables narrowband infrared detection at 2096 nm and high-sensitivity CO_2 sensing via a photo-assisted approach.

I anticipate that this work is very interesting, and will have high academic impact for the development of upconversion luminescent materials and high-performance optoelectronic devices. Furthermore, the manuscript is well-structured and clearly presented; therefore, I recommend it for publication in Nature Communications. A few minor points are listed below:

(Q1) Machine learning: What nearest-neighbor search strategy does the algorithm employ during the numerical screening stage? When no satisfying nearest neighbor or valid combination exists, what is the algorithm's fault-tolerance mechanism?

Response: We sincerely thank the reviewer for your comment. This algorithm employs a nearest value search strategy based on linear traversal and threshold constraints during the numerical screening stage. During execution, the algorithm performs a complete sequential traversal of the target numerical column, calculating the absolute deviation between each numerical value and a preset target value one by one. Among all candidate values whose deviations do not exceed the specified threshold, the value with the smallest deviation from the target is selected as the final nearest value, serving as the reference point for subsequent combination calculations and index solving. This search strategy offers three significant advantages: First, it is simple to implement and highly robust, requiring no complex data preprocessing and being directly applicable to small-scale numerical sequences, whether ordered or unordered. Second, the matching accuracy is controllable; the threshold parameter flexibly defines the valid matching range, preventing outliers and invalid values from interfering with the results. Third, the computational efficiency is relatively high, as the algorithm requires only a single linear traversal to complete the search, resulting in low time complexity, which ensures good execution performance and practicality in engineering applications.

Furthermore, the algorithm incorporates a well-designed two-level fault-tolerant mechanism to guarantee the robustness of the overall process and the standardization of output results. When no nearest value satisfying the threshold condition exists in the numerical sequence, the algorithm immediately terminates the subsequent combination calculation process for the current material and returns an empty result set, thereby avoiding invalid computations and error propagation. When a valid nearest value exists but no numerical combination meeting the required rules can be identified, the algorithm automatically fills in a unified placeholder, ensuring that output fields for different materials remain complete and uniformly formatted. This prevents program interruption or output anomalies due to the absence of results for certain data, providing a stable and reliable data foundation for subsequent data organization, result analysis, and system integration.

These detailed discussion of the machine learning algorithms mentioned above have been

added to the Supplementary Note 2 in Supplementary Information.

(Q2) This LEGO-stacking single-photon upconversion model is generalizable. The authors should establish upconversion rate equations to verify which factors the emission enhancement depends on.
Response: We thank for your good suggestion. Following your suggestion, we have supplemented this LEGO-stacking single-photon UC rate equation based on rare-earth ions to qualitatively understand the enhanced UC photophysical mechanism. Referring to the energy level configuration of RE^{3+} in Fig. 1b of the manuscript, we obtained that the energy level emission intensity (I_{RE}) can be calculated from the population density of N_2 state:

$$I_{RE} = R_2 N_2 = \frac{N_0 \sigma_{01} \sigma_{02} \rho^2}{R_1} \quad \text{(R1)}$$

where N_0, N_1, and N_2 denote the population densities of RE^{3+} energy levels. R_1 and R_2 are the radiative rates of RE^{3+}. ρ is the laser photon number density. σ_{01} and σ_{02} denotes the absorption cross-section of RE^{3+} energy levels. It can be concluded from Equation.7 that the emission intensity of RE^{3+} is proportional to σ_{01}, σ_{02}, ρ and inversely proportional to the R_1, which means that the excitation photon density, absorption cross-sections and lifetimes of the energy levels play a important role in single-photon UC systems with photo-assisted resonance. These detailed analyses have been incorporated into the manuscript and Supplementary Note 1 in Supplementary Information.

(Q3) Under cascade pumping, the red emission intensity enhancement factor (×4220) of the $NaYS_2$:1%Ho^{3+} system is significantly higher than that of other Ho^{3+} singly doped systems with different concentrations. The paper should clarify why the $NaYS_2$:1%Ho^{3+} system exhibits a higher enhancement factor.
Response: We sincerely thank the reviewer for your comment. In response to the reviewer's concern regarding why the $NaYS_2$:1%Ho^{3+} system exhibits a significantly higher enhancement factor under cascade pumping, we have conducted experiments to compare the luminescence enhancement behavior across different Ho^{3+} doping concentrations (Fig. S7). The results confirm that this selective enhancement effect persists consistently across various Ho^{3+} concentrations. An appropriate doping concentration not only ensures sufficient absorption but also effectively suppresses detrimental energy back-transfer and cross-relaxation processes among the ions, which are complex and often lead to undesirable energy losses. Therefore, the $NaYS_2$:1%Ho^{3+} system achieves the optimal balance, resulting in a much higher red emission intensity enhancement factor (×4220) than other Ho^{3+} singly doped systems with different concentrations. These detailed analyses have been incorporated into the manuscript.

(Q4) The long-term stability data of the photoresponse devices are of positive significance. The authors should supplement the changes in photocurrent values of the upconversion PDs under prolonged illumination, which would help verify its robustness in practical applications.
Response: We greatly appreciate the reviewer's insightful comment on the long-term robustness of our UC PDs, which is indeed a key requirement for practical deployment. Below we provide a detailed response supported by the stability data presented in **Figure R5** (**Corresponding to the Fig. S30**) in Supplementary Information, which demonstrate the excellent operational and environmental stability of our PDs:

Operational stability under prolonged periodic illumination (2000 s)

To assess the stability of device under continuous, repeated light excitation, we performed cyclic on/off illumination tests using 980 nm (20 mW·cm^{-2}) and 2096 nm light (40 mW·cm^{-2}) over a 2000-second duration (**Figure R5a** (**Corresponding to the Fig. S30a**)). The device exhibits highly repeatable and stable photoresponse behavior throughout the entire measurement period. As clearly shown in the plot, the peak photocurrent amplitude remains nearly unchanged across all on/off cycles, with no observable decay in signal magnitude over 2000 s of continuous operation. The negligible fluctuation in photocurrent (well within the noise level of the measurement system) confirms that our PDs maintain consistent performance under prolonged periodic illumination, verifying their excellent operational stability.

Device-to-device reproducibility

To evaluate the consistency of our fabrication process, we prepared 20 independent PDs under identical conditions. As shown in **Figure R5b** (**Corresponding to the Fig. S30b**), the normalized responsivity of all devices falls within a narrow range of ±10% relative to the average value, confirming good batch-to-batch reproducibility and low performance variation across different devices.

Collectively, these results confirm that our UC PDs exhibit both outstanding operational stability under continuous illumination and robust reproducibility, which are essential prerequisites for practical applications. We have added detailed descriptions and discussions of these stability results in the revised manuscript (page 12).

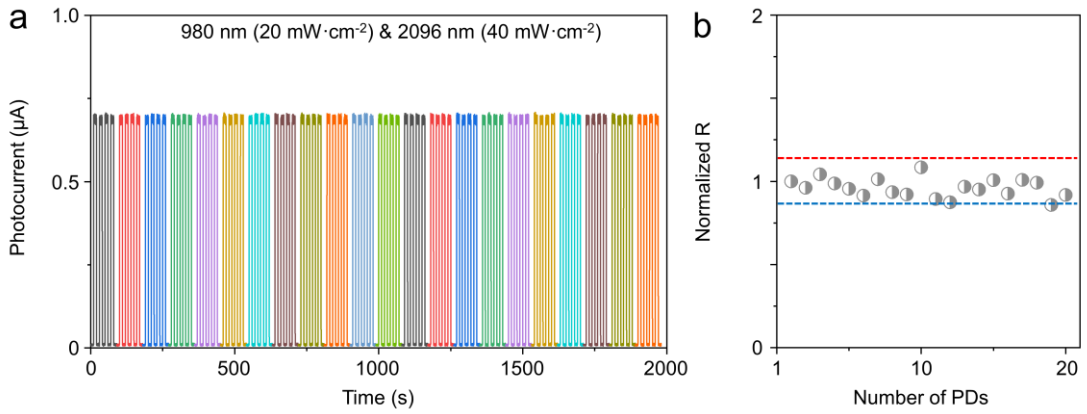

Figure R5 (**Corresponding to the Fig. S30**) (a) Cyclic on/off illumination tests using 980 nm (20 mW·cm^{-2}) and 2096 nm light (40 mW·cm^{-2}) over a 2000-second duration. The peak photocurrent amplitude remains nearly unchanged across all on/off cycles, with no observable decay in signal magnitude over 2000 s of continuous operation (b) The normalized *R* of the prepared 20 independent PDs under identical conditions. The normalized *R* of all devices falls within a narrow range of ±10% relative to the average value.

(Q5) The gas detection application is based on laser absorption spectroscopy, using a CO_2/N_2 gas mixture. The authors should also provide the absorption curve of N_2 to demonstrate that it exhibits no significant absorption at 2004 nm.

Response: We greatly appreciate the reviewer's valuable comment. We fully agree with this point, and have added the absorption spectra of both CO_2 and N_2 in the range of 1800-2200 nm (**Figure R6** (**Corresponding to the Fig. S31**)) to explicitly demonstrate the negligible absorption of N_2 at the target wavelength of 2004 nm. The blue curve in the added figure corresponds to CO_2, which shows strong, characteristic absorption peaks centered at ~2004 nm. These sharp peaks arise from

the infrared-active vibrational-rotational transitions of linear CO_2 molecules, which form the basis of our laser absorption spectroscopy detection. The red curve shows the absorption signal of pure N_2. To make the baseline visible, the N_2 signal has been scaled up by a factor of 10^{11}. Even with this extreme magnification, N_2 exhibits no detectable intrinsic absorption across the entire 1800-2200 nm range, including the 2004 nm target wavelength. Thus, N_2 in the gas mixture will not produce any spectral interference with the CO_2 measurement at 2004 nm. We have added this figure and the corresponding explanation in the revised manuscript and Supplementary Information for clarity.

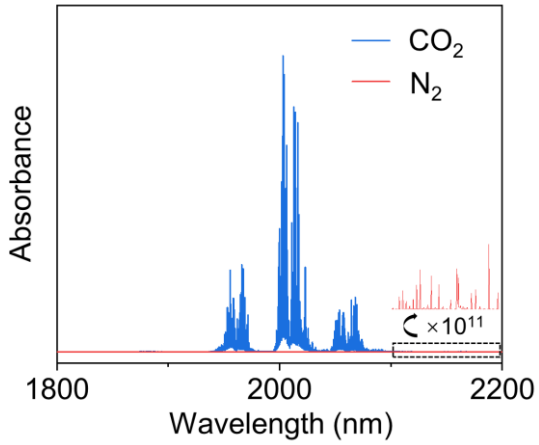

Figure R6 (**Corresponding to the Fig. S31**) Absorption of CO_2 and N_2 gas ranging from 1800 nm to 2200 nm. The strong absorption of CO_2 contrasts sharply with the extremely weak absorption of N_2, with a difference exceeding 11 orders of magnitude. N_2 causes virtually no interference in the characteristic absorption band of CO_2, enabling high-sensitivity quantitative detection of CO_2 concentration by monitoring the absorption peak near 2004 nm.

Response to Reviewer #3:

Reviewer #3: This work describes a dual wavelength excitation approach to achieve high efficiency emission from upconversion materials at discrete red/green and blue wavelengths. The authors claim to use a machine learning approach to inform the ideal combinations of excitation wavelength to produce optimal emission at the each wavelengths. They then go on to experimentally validate their predictions and demonstrate the application of their dual wavelength excitation methodology for gas and CO2 sensing in combination with suitable photodetectors.

The work is certainly interesting and presents a simple and elegant approach to achieving efficient visible light emission from upconverting (UC) lanthanide ions. It constitutes a significant advancement in the field of photon UC with broad applicability into other disciplines. I therefore recommend publication in Nature Communications after some minor revisions.

(Q1) The machine learning algorithm in Supp Note 1 needs more thorough description and referencing. For example, the statement "…a simple transformation is performed using machine learning algorithms to calculate the corresponding gaps of energy levels." is vague and uninformative.

Response: We appreciate the careful comment. According to your suggestion, in the revised Supplementary Note 2, we have comprehensively supplemented and refined the detailed description of the adopted machine learning algorithm. We have further elaborated the nearest neighbor search strategy adopted by the algorithm in the numerical screening process, as well as its technical advantages in efficient data matching and rapid parameter screening. Meanwhile, we added the specific fault-tolerance mechanism of the algorithm when there are no qualified nearest neighbor values or valid material parameter combinations. In addition, relevant literature references closely related to this algorithm strategy have been supplemented to enhance the rationality and credibility of the method.

The revised content has made the algorithm principle, implementation process and functional characteristics more complete and understandable, avoiding vague descriptions as mentioned in the original manuscript.

(Q2) In general it would have been good to increase the discussion around the minimum requirements in the lifetimes of the excited state to function as "virtual ground states". What is this threshold? Are the reported pathways the only possible combinations to produce emission in the RBG regions or are other less efficient pathways also viable?

Response: Thank you for these constructive and valuable comments. We agree with your suggestion that the lifetime threshold for functioning as "virtual ground states" is important for understanding the UC populating process in our system. Indeed, the lifetime of an intermediate excited state is a key prerequisite to serve effectively as a virtual ground state. The "threshold" can be determined by the competition between two processes: (i) the decay rate of the intermediate state (radiative and non-radiative transitions, which deplete the virtual ground state population), and (ii) the excitation rate R_{pump} of the second pump laser (which drives the population from the virtual ground state to the target emitting level).

For the intermediate state to accumulate sufficient population to enable the second excitation step, its lifetime $\tau_{intermediate}$ would satisfy：

$$\tau_{\text{intermediate}} \geq \frac{1}{R_{\text{pump}}} \tag{R2}$$

where R_{pump} is the effective excitation rate of the second pump laser. Theoretically, in typical rare-earth-doped systems, the intrinsic long lifetime of 4f-4f transitions (typically on the order of microseconds to milliseconds) together with practical pump intensities ensures that the "virtual ground state" condition is generally satisfied as long as the excited-state lifetime exceeds several microseconds.

We further performed cascade pumping experiments on $NaHoS_2$ (100% Ho^{3+}), as shown in **Figure R7, corresponding to Fig. S18**. This system exhibits a shorter lifetime (2.2 ms) due to concentration quenching. It is observed that $NaHoS_2$ also shows enhanced red emission under cascade pumping. The enhancement factor decreases from ~4220-fold for the 1% Ho^{3+} sample to only 22-fold for the 100% Ho^{3+} sample. Such enhancement can be achieved in $NaYF_4$, Y_2O_3 and $La_2Mo_2O_9$, which have lifetimes on the order of microseconds. However, because such a threshold can be affected by many factors, it is difficult to quantify and determine a specific value for rare earth ion doped luminescent systems.

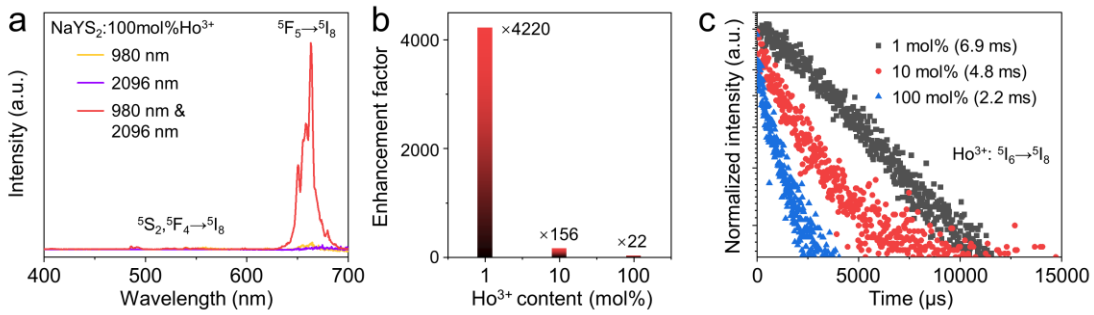

Figure R7 (Corresponding to the Fig. S18) (a) The UC emission spectra of $NaHoS_2$ under single/dual-wavelength excitation. (b) Histogram of enhancement factor with various Ho^{3+} concentration (1, 10, 100 mol%) under dual-wavelength excitation. (c) The normalized decay curves of $^5I_6$ (Ho^{3+}) energy levels with various components of Ho^{3+}. The intermediate-state lifetime exhibits a positive correlation with the enhancement of cascade-pumping UC luminescence, i.e., a longer excited-state lifetime is more favorable for effectively serving as a virtual ground state to facilitate re-excitation, thereby enabling efficient cascade pumping UC.

Regarding the second question, the pathways reported in our manuscript are not the only combinations that can achieve RGB emission; other effective and feasible pathways also exist when using a pump wavelength precisely matched to the energy gap of Ho^{3+}. According to your suggestion, we performed additional experiments using co-excitation of 980 nm and 1208 nm, observing clear green and red UC enhancement, which is consistent with the cascade pumping mechanism (**Figure R8a; corresponding to Fig. S14a**). When using 1532 nm and 1208 nm, only a twofold improvement was identified for red emission (**Figure R8b; corresponding to Fig. S14b**). This is because these pump wavelengths are not ideally matched to the energy gaps of Ho^{3+}. Then, when the deviation between the pump wavelength and the energy gap becomes larger when employing 980 nm and 1532 nm, UC luminescence enhancement disappears (**Figure R8c; corresponding to Fig. S14c**), highlighting the critical role of precise energy-gap matching in this

scheme.

We have incorporated these additional experimental results and related discussions into the revised manuscript (page 6, 7) and Supplementary Information.

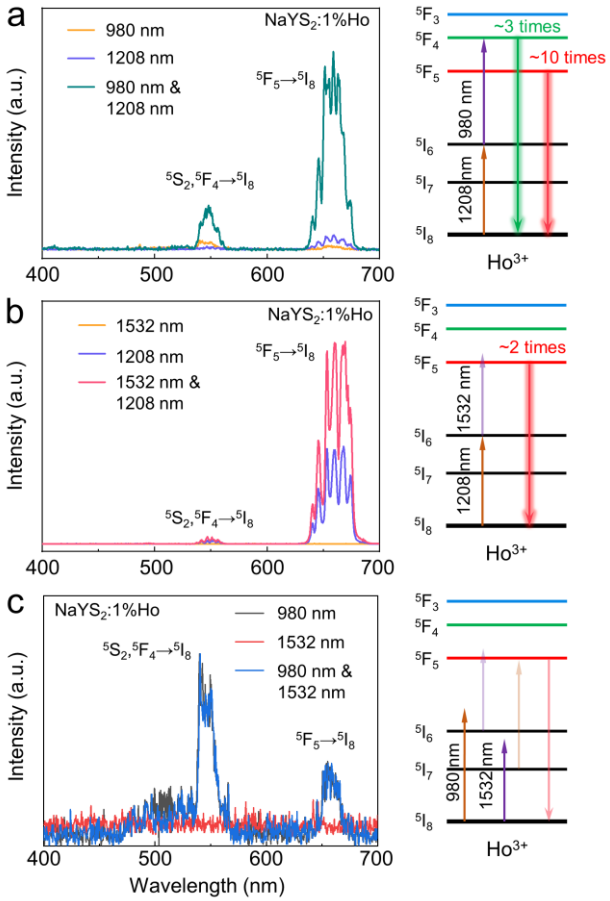

Figure R8 (**Corresponding to the Fig. S14**) UC emission spectra of $NaYS_2$:Ho^{3+} (1 mol%) under various single/dual-wavelength excitation ((a) 980 nm and 1208 nm; (b) 1208 nm and 1532 nm; (c) 980 nm and 1532 nm), accompanied with a simple transition mechanism of single-photon UC by LEGO-inspired photon stacking.

(Q3) Enhancement factors are often reported, but it is not always clear what they are in reference too. Fig S6 in particular was not clear.

Response: We thank the reviewer for pointing out the unclear description of the reference baselines for the enhancement factors in Figure S6. According your comment, we provide a detailed explanation of the figure as follows: In Figure S6, all enhancement factors are calculated with the Ho^{3+} UC emission intensity under dual-wavelength cascade excitation (λ_{ex} = 980 nm & 2096 nm) as the numerator, and the denominator corresponds to three different reference conditions. Specifically, the bars for purple and blue represent the enhancement factor of the cascade excitation relative to 980 nm excitation, to 2096 nm excitation, and the red bars represent the enhancement factor relative to sum of the intensities under the two single-wavelength excitations.

To avoid any ambiguity, we have added clear figure captions in both the revised manuscript (page 5) and the Supplementary Information (Figures S6 and S12), completely eliminating any potential confusion.

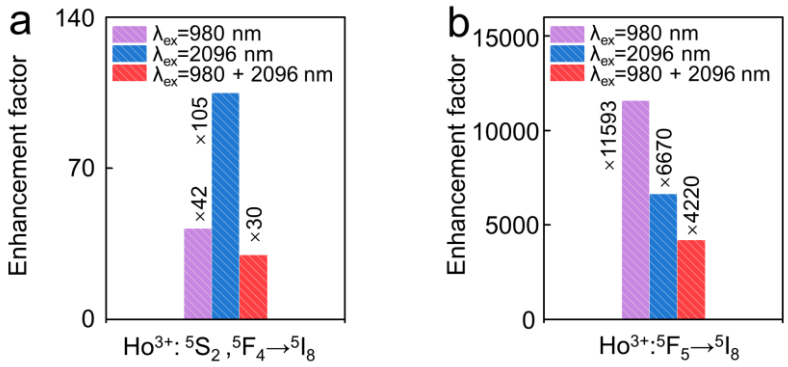

Figure R9 (**Corresponding to the Fig. S6**) Histogram of various emission (a: $^5S_2$,$^5F_4$→$^5I_8$; b: $^5F_5$→$^5I_8$) enhancement factor in Ho^{3+} single-doped $NaYS_2$ under dual-wavelength cascade pumping. Under cascade excitation at 980 nm and 2096 nm, the green emission intensity (Ho^{3+}: $^5S_2$,$^5F_4$→$^5I_8$) is 42 times that under 980 nm alone, 105 times that under 2096 nm alone, and 30 times the sum of the two single excitations. For the red emission (Ho^{3+}: $^5F_5$→$^5I_8$), the cascade excitation yields intensities enhancements of 11593, 6670, and 4220 times corresponding to the respective single excitations and their sum.

(Q4) The scheme and description of the gas sensing setup is misleading. The reference and detection beams do not produce a new converging pink photon, but rather travel colinear toward the photodetector. The structure of the photodetector, including the deposition of the UC crystals is not suitably described in either the text or SI.

Response: We sincerely thank the reviewer for the careful comments. According to your suggestion, we revised the gas sensing setup, as shown in revised **Figure R10** (**Corresponding to the Fig. 4a**). It can be seen that the reference light and detection light are collinear and propagate together to the PDs, with no new photons generated throughout the process. We have now thoroughly optimized the optical path color scheme and labeling, and removed all potentially misleading visual elements to accurately represent the actual collinear dual-beam propagation configuration.

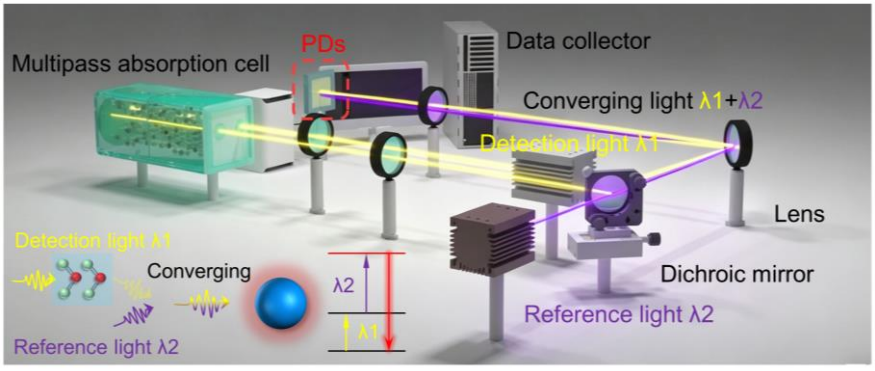

Figure R10 (**Corresponding to the Fig. 4a**) LAS gas sensing based on dual-wavelength cascade pumping narrowband NIR optical detection.

We further performed the structure characterization for the PDs. Cross-sectional top and side views of the PDs are shown in **Figure R11** (**(corresponding to Fig. S24**). In addition, the detailed

textual descriptions have been provided in Supplementary Note 6, fully describing the overall device structure, the deposition method of the UC crystal, its distribution characteristics, and the relevant fabrication parameters. These additions clearly elucidate the loading configuration of the UC crystal on the detector surface, supplementing the previously missing structural details.

All the above revisions have been highlighted in the revised manuscript.

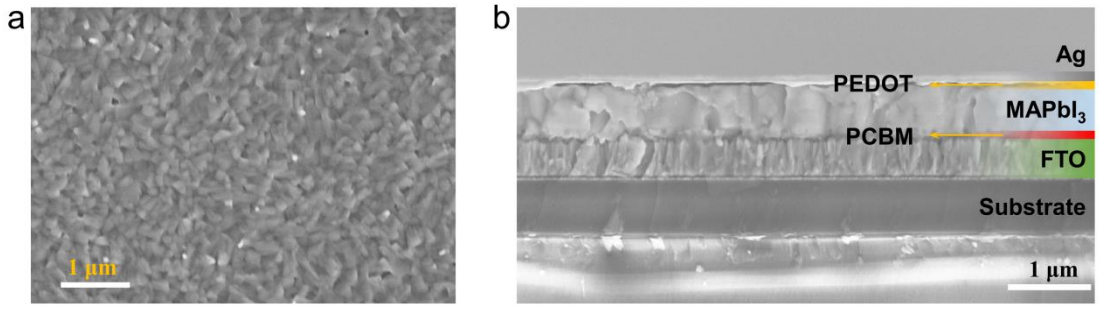

Figure R11 (**Corresponding to the Fig. S24**) (a) Top view SEM image of the perovskite structured $MAPbI_3$ hybrid film. (b) Side view SEM image of PDs. The PDs structure, from bottom to top, consists of a glass substrate, a FTO transparent conductive electrode, PCBM electron transport layer, a $MAPbI_3$ perovskite absorber layer, PEDOT hole transport layer, and Ag top electrode. The yellow arrows indicate the positions of the PCBM and PEDOT layers, respectively. The scale bar corresponds to 1 μm, providing a reference for estimating the thickness of each layer. The $MAPbI_3$ perovskite layer exhibits dense and continuous grains, with clear and uniform interfaces between adjacent layers, confirming the high-quality film deposition and good interlayer contact in the fabricated device.

(Q5) Can the authors explain the origin of the reported EQE exceeding 100%?

Response: Thank you very much for your insightful question regarding the origin of the external quantum efficiency (*EQE*) exceeding 100%. The calculation formula for the EQE of a detector is as follows:

$$EQE = R\frac{hc}{\lambda e} \tag{R3}$$

where h, c, and e are both constant, representing Planck's constant, light velocity, and elementary charge. In fact, our PDs are pumped under co-excitation of 980 nm and 2096 nm, where 2096 nm is the detected light and 980 nm serves as an auxiliary reference light. Therefore, when evaluating the *EQE* for 2096 nm, we used the *EQE* measured under co-excitation of 2096 nm and 980 nm (without considering the energy of 980 nm) and subtracted the *EQE* measured under 980 nm excitation alone.

On the other hand, the presence of the 2096 nm beam enables the intense 980 nm pump to excite electrons to even higher energy levels, as evidenced by the enhanced green and blue emissions (Fig. 1e). These additional visible photons increase the total visible photon yield, thereby further raising the measured quantum efficiency (**Fig. S26**).

(Q6) In general, reported for photodetection and CO_2 sensing appear idealised examples and lack evidence of repetition or error ranges.

Response: Thank you very much for this constructive comment. According to your suggestion, we supplemented robust stability and repeatability data of our UC PDs for CO_2 sensing, as elaborated

below:

Operational stability under continuous illumination

To assess the device's stability under continuous, repeated light excitation, we performed cyclic on/off illumination tests using 980 nm (20 mW·cm^{-2}) and 2096 nm light (40 mW·cm^{-2}) over a 2000-second duration (**Figure R5a** (**Corresponding to the Fig. S30a**)). The device exhibits repeatable and stable photoresponse behavior throughout the entire measurement period. As clearly shown in the plot, the peak photocurrent amplitude remains nearly unchanged across all on/off cycles, with no observable decay in signal magnitude over 2000 s of continuous operation.

Device-to-device reproducibility

To evaluate the consistency of our fabrication process, we prepared 20 independent PDs under identical conditions. As shown in **Figure R5b** (**Corresponding to the Fig. S30b**), the normalized responsivity of all devices falls within a narrow range of ±10% relative to the average value, confirming good batch-to-batch reproducibility and low performance variation across different devices.

We have added detailed descriptions and discussions of these stability results in the revised manuscript (page 12) and Supplementary Information.

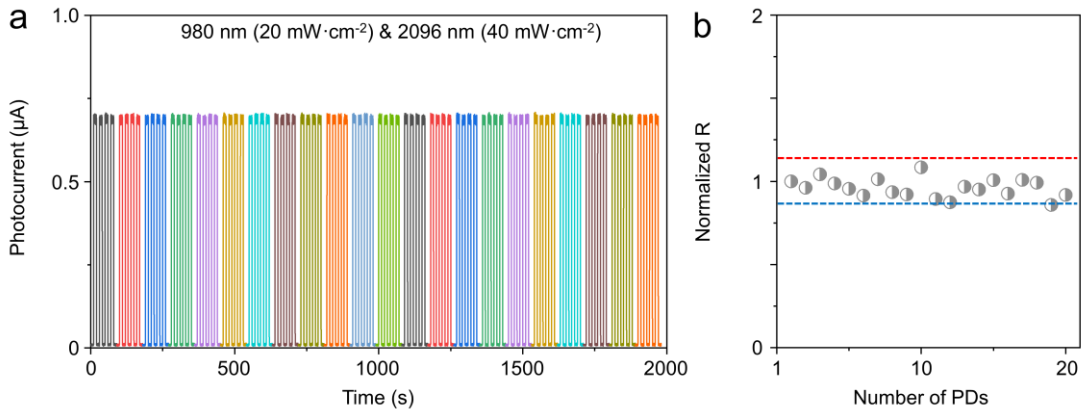

Figure R5 (**Corresponding to the Fig. S30**) (a) Cyclic on/off illumination tests using 980 nm (20 mW·cm^{-2}) and 2096 nm light (40 mW·cm^{-2}) over a 2000-second duration. The peak photocurrent amplitude remains nearly unchanged across all on/off cycles, with no observable decay in signal magnitude over 2000 s of continuous operation (b) The normalized *R* of the prepared 20 independent PDs under identical conditions. The normalized *R* of all devices falls within a narrow range of ±10% relative to the average value.

(Q7) Minor grammatical errors including undefined acronyms (Eg. PD, PCBM) and experimental details are not sufficient for replication (Eg. Excitation intensities in Fig 1e-g and Fig 2h-j, description of the commercial 2004 nm PD used for comparison, etc.)

Response: We greatly appreciate the reviewer's careful and constructive comments. According to your comments, we have now fully revised the manuscript as follows:

Grammar and acronym issues: All grammatical errors have been corrected, and every acronym (including PDs (photodetectors), PCBM ([6,6]-phenyl-C61-butyric acid methyl ester) and PEDOT (poly (3,4-ethylenedioxythiophene) polystyrene sulfonate)) is now explicitly defined at its first appearance in the text.

Experimental details for replication: We have added the specific excitation power for Fig. 1e-g and Fig. 2h-j in the corresponding figure captions.

We have supplemented the full specifications of the commercial 2004 nm PDs (including model number, manufacturer) used for comparison in Supplementary Note 4. The 2004 nm detector chip, supplied by INP Photonics (Suzhou) Co., Ltd., is a photodiode designed for carbon dioxide sensing applications, model number INP-PCS-2004N-A09-01. It operates within a wavelength range of 900-2200 nm and a temperature range of -40 to 80 ℃.

All revisions are clearly marked in the revised manuscript. Thank you again for your rigorous review, which has greatly enhanced the scientific rigor of our work.